J Mol Model (2008) 14:417–425
DOI 10.1007/s00894-008-0288-x

ORIGINAL PAPER

Theoretical study of the novel sandwich compound $[Au_3Cl_3Tr_2]^{2+}$

Jesús Muñiz · Luis Enrique Sansores · Ana Martínez · Roberto Salcedo

Received: 27 September 2007 / Accepted: 8 February 2008 / Published online: 15 March 2008

Abstract A theoretical study of a sandwich compound with a metal monolayer sheet between two aromatic ligands is presented. A full geometry optimization of the $[Au_3Cl_3Tr_2]^{2+}$ (1) compound, which is a triangular gold(I) monolayer sheet capped by chlorines and bounded to two cycloheptatrienyl (Tr) ligands was carried out using perturbation theory at the MP2 computational level and DFT. Compound (1) is in agreement with the 18–electron rule, the bonding nature in the complex may be interpreted from the donation interaction coming from the Tr rings to the Au array, and from the back-donation from the latter to the former. NICS calculations show a strong aromatic character in the gold monolayer sheet and Tr ligands; calculations done with HOMA, also report the same aromatic behavior on the cycloheptatrienyl fragments giving us an insight on the stability of (1). The Au –Au bond lengths indicate that an intramolecular aurophilic interaction among the Au(I) cations plays an important role in the bonding of the central metal sheet.

Keywords Aurophilic interactions · Monolayer sheet · NICS calculations

Introduction

The study of metallocenes has been widely explored since the discovery of ferrocene [1]. Metallocenes form sandwich compounds where a metal atom is surrounded by two aromatic carbocyclic ligands (benzene, cyclopentadienyl), which in some cases possess catalytic properties. Although several such complexes have been achieved [2], only a small group of sandwich compounds with a metal monolayer sheet between the two carbocyclic ligands has been synthesized. For instance, $Ni_3(benzene)_2$ was found in $Ni_n(benzene)_m$ clusters in gas phase using laser vaporization [3]. Theoretical studies based on the density functional theory have been carried out to test the stability of sandwich compounds with a transition metal atom [4, 5] and also, extended-Hückel theory has been used to predict the existence of sandwich compounds with a metal monolayer sheet [6]. More recently [7], the synthesis of the discrete metal monolayer sandwich compounds $[Pd_3(C_7H_7)_2Cl_3][PPh_4]$ and $[Pd_5(naphthacene)_2$ (toluene)$][B(Ar_f)_4]_2$ (4–toluene), with $B(Ar_f)_4 = B[3,5(CF_3)_2C_6H_3]_4$ have been reported. The first of these two compounds is a tripalladium complex capped by chlorines between two cycloheptatrienyl ligands, which has shown promising catalytic properties. The second one is a pentapalladium sheet with a triangle-trapezoid geometry between two naphtacene rings. Both compounds have been studied by DF theory considering the simplified models $[Pd_3Tr_2Cl_3]^-$ and $[Pd_5(naphthacene)_2]^{2+}$. It was found that there is an electron donation from the ligands to the metal sheets and then a back-donation from the metal species to the ligands.

The finding of the Pd compounds has opened a new field in the search of other metal elements that can be used in the monolayer metal sandwich chemistry, since these molecular systems can be the building blocks of bulk systems like unsaturated hydrocarbons adsorbed on metallic surfaces [7].

The chemistry of sandwich compounds can be extended to gold monolayer sheets, since gold has shown to be a flexible metal when coordinated with other gold atoms [8], giving rise to a phenomenon termed aurophilicity. Auro-

J. Muñiz (✉) · L. Enrique Sansores · A. Martínez · R. Salcedo
Instituto de Investigaciones en Materiales,
Universidad Nacional Autónoma de México,
Apartado Postal 70–360,
México, México DF 04510, México
e-mail: jesus@iim.unam.mx

philicity has been the subject of several experimental and theoretical works [8–11]. It is mainly characterized by an Au–Au bond length contraction ranging from 300 to 360 pm; this bond length is smaller than the van der Waals radii for gold. The aurophilic bonding energy is like the strongest hydrogen bonds or the weakest covalent bonds, i.e., the aurophilic interaction energy ranges from (5–15) kcal mol^{-1} [12–14]. Theoretical studies have also been carried out to show that the aurophilic interaction is originated by relativistic and correlation effects [15–18].

The synthesis of a sandwich compound with a gold monolayer sheet has not been reported and a theoretical study of such kind of compounds is not available. The aim of this work is to calculate by quantum methods, the geometry and electronic structure of a novel sandwich compound with a monolayer sheet, as well as to predict the existence of possible catalytic properties of the compound.

Computational method

The geometry optimization was performed with the MP2 computational method [19], which accounts for explicit dispersion effects. LANL2DZ small-core pseudopotential with 19 valence electrons was used for the Au atoms to include relativistic effects [20]. The Stuttgart small-core pseudorelativistic effective core potential [21] with 19 valence electrons was also used for Au, with the optimized contracted Gaussian basis set of Schäfer et al. [22]: The valence triple-ζ plus one polarization type, TZVP. This basis set was augmented with two additional f – type polarization functions (α_f=0.2, 1.19), which were calculated by Pyykkö et al. [23]. The former function is a diffuse f orbital necessary for the intermolecular interaction, and the latter, important for the Au d^{10} correlation, is a compact f orbital which acts as a polarization function in intramolecular bonding. The basis sets for the calculations where LANL2DZ basis set for Au and the 6–31 ++G** [24, 25] for the other atoms are used will be referred to as B1; those computations where the basis TZVP for Au and the 6–31 ++G** are employed will be denoted by B2. Charge calculations were carried out in accordance with the NBO method [26].

The geometry of complex 1 was also fully optimized by DF Theory using the following approaches: (a) The Xα exchange potential given by Slater [27–29], considering the parameter α=0.7, (b) the functional suggested by Vosko, Wilk and Nusair (VWN), including a correction on local correlation [30], and (c) The VWN functional combined with the gradient corrected exchange potential of Becke of 1988 [31], given in accordance with GGA, and the Perdew's non-local correlation potential of 1986 [32], which is defined with a gradient correction. The latter approach will be denoted as VBP.

In all DFT calculations, the inner core shells were kept fixed to reduce the computational cost [33]. The shell [$1s^2$] was frozen for C, [$1s^2$–$2p^6$] for Cl and [$1s^2$–$4d^{10}$] for Au. The Dirac method [34] was applied to compute the atomic core orbitals; once obtained, they were kept unrelaxed in compound (1).

In the chemistry of gold, specifically the aurophilic interaction, relativistic effects play an important role. Therefore, in all DFT computations, the scalar relativistic zero-order regular approximation (ZORA) [35, 36] was used, where an average of the spin-orbit splittings is taken into account. Explicit spin-orbit effects were not considered since they are not important on Au(I) systems [37]. All calculations were preformed using a Slater type orbital basis set: The high quality triple –ζ plus one polarization basis set (STO–TZP). The aromatic character of compound (1) was quantified by NICS calculations in accordance with Schleyer's method [38] and HOMA [39]. MP2 and DFT calculations were performed using GAUSSIAN 03 [40] and the Amsterdam density functional package (ADF 2006) [34, 41, 42], respectively.

Results and discussion

Structural description

The gold sandwich compound $[Au_3Cl_3Tr_2]^{2+}$ was fully optimized by the MP2 computational method with the B1 and B2 basis sets, using no symmetry constraints; the complex is in agreement with the 18-electron rule. The optimized structure (see Fig. 1) is a true minimum since a vibrational analysis revealed that all frequencies are real. The optimized parameters are presented in Table 1; the calculated structure is a trigold cluster, where every gold is bonded to a chlorine atom, which is sandwiched by two tropylium (Tr) rings. The Tr rings present a staggered and eclipsed geometry using the B1 and B2 basis sets, respectively. Both rings are slightly deviated from the plane; the tilt angles of the upper (Tr1) and lower (Tr2) tropylium rings with respect to the $[Au_3Cl_3]$ fragment are reported in Table 1. The rings are certainly bound to the central gold sheet, since the Au – C bond distances range from 228 to 237 pm (at the MP2/B1 level), and from 220 to 230 pm (at the MP2/B2 level). Similar bond lengths have been reported in the analogous $[Pd_3Cl_3Tr_2]^-$ [7] sandwich compound. The Au–Au bond lengths inside the gold central cluster (283–296 pm at the MP2/B1 level and 271–282 pm at the MP2/B2 level) are smaller than the van der Waals bond distance of 360 pm. This could be associated with the presence of aurophilic interactions inside the central cluster.

The aurophilic interaction has been analyzed considering the empirical relation proposed by Herschbach and Laurie [43], where the force constants (in N/cm) and the Au–Au

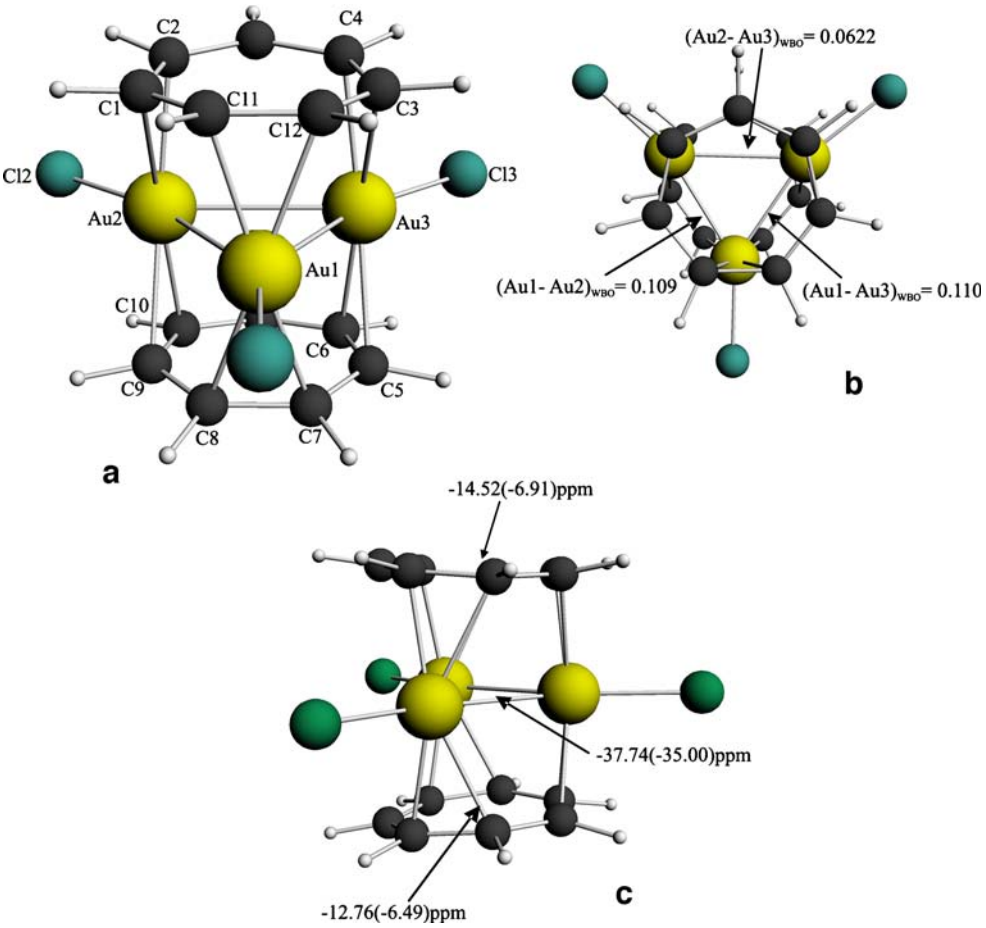

Fig. 1 (**a**) Ground state geometry of complex **1**; (**b**) Top view of compound **1** and Wiberg bond orders computed with the MP2/B1 computational method; (**c**) Lateral view of compound **1** and NICS values calculated with the MP2/B1 method; the values in parenthesis were obtained at the VWN/TZP level

bond lengths (in pm) are related by the following expression; which works in the range [247–355]pm

$$R_{Au-Au} = 268pm + 29 \cdot \ln([N/cm]/k_{Au-Au}) \quad (1)$$

where $R_{Au\text{-}Au}$ and $k_{Au\text{-}Au}$ are the Au–Au bond distances and the Au–Au force constants, respectively. The calculated $k_{Au\text{-}Au}$ on the trigold(I) complex amounts to 0.35 N/cm at the MP2/B1 level. When this value is given in Eq. (1), a value of 298.1 pm for the Au–Au distance is returned, in reasonable agreement with the calculated distance of 283 pm. This indicates that an aurophilic bonding is certainly formed on the trigold(I) ring of complex (1). The latter assumption can also be supported by the Wiberg bond order [44] results (see Fig. 1); this scheme is handled in the current work since it has shown to be reliable when implemented on transition metal complexes [7]. From Fig. 1, all the Wiberg bond orders are non-zero and greater than 0.06; this can also be addressed to the presence of an aurophilic bonding on the Au ring, since the computed bond order in the $(Au^{+})_2$ cation is zero.

It is known that dispersion effects rule the aurophilic interactions and ab initio correlation corrected methods such as MP2 adequately reproduce the aurophilic bonding; nevertheless, it has been recently shown by Wang et al. [45] that the use of local density functional methods gives reasonable equilibrium bond lengths and bond energies where the closed-shell Au(I) interactions are involved. Taking the latter into account, the use of local density functionals for the electronic structure calculations was considered in the present work.

Full geometry optimizations obtained with DFT at the Xα/TZP, VWN/TZP and VBP/TZP levels were also performed. Optimized bond lengths are presented in Table 1: The Au–Au bond lengths are in the range of aurophilic interactions; slightly stronger aurophilic bonds than those found at the MP2 level were obtained. The Au–C bond lengths distances average 227.3 pm at the VWN/TZP level, i.e., the distances between the central gold cluster and the upper Tr ligand, while the average Au–C distances between the trigold compound and the lower Tr ligand amounts to 227.1 pm. The Tr ligands also underwent a slight deviation from the plane, which is consistent with the results found by the MP2 computational method.

Charge distribution

In order to understand the bonding nature of the complex under study, the electron populations of the building fragments were calculated at singlet state at the MP2/B1 level to

Table 1 Optimized bond lengths (pm) and tilt angles (deg) of compound **1**

Bond	Bond distance MP2/B1	Bond distance MP2/B2	Bond distance X Alpha/TZP	Bond distance VWN/TZP	Bond distance VBP/TZP
Au1 – Au2	282.8	271.0	276.9	275.1	292.4
Au1 – Au3	282.6	268.7	275.8	275.2	277.9
Au2 – Au3	296.8	281.7	302.7	297.0	316.6
Au1 – C11	218.2	221.7	223.0	221.4	228.6
Au1 – C12	269.7	224.7	224.5	224.4	232.6
Au1 – C7	233.2	225.5	223.5	222.4	230.3
Au1 – C8	234.5	230.1	223.8	222.8	228.9
Au2 – C1	264.4	219.8	237.0	236.4	263.1
Au2 – C2	227.7	284.0	227.9	224.1	240.9
Au2 – C9	260.6	257.7	234.2	231.6	254.3
Au2 – C10	237.0	226.4	229.4	226.6	243.6
Au3 – C3	261.0	221.3	231.4	230.7	233.6
Au3 – C4	229.2	277.6	231.6	226.7	270.4
Au3 – C5	261.0	261.1	232.6	233.4	233.1
Au3 – C6	236.0	225.6	230.6	225.7	269.0
Au1 – Cl1	243.4	236.9	233.2	232.0	238.3
Au2 – Cl2	241.0	232.1	231.5	231.1	232.5
Au3 – Cl3	241.0	232.1	231.7	231.2	232.5
[1][Au_3Cl_3]-Tr1	227.4	222.2	219.9	212.2	227.4
[1][Au_3Cl_3]-Tr2	238.1	214.0	221.3	201.6	234.0
Tilt Angles					
[Au_3Cl_3]-Tr1	9.2	18.8	5.1	4.7	9.4
[Au_3Cl_3]-Tr2	5.5	2.8	4.2	3.1	9.5

[1] These bond lengths correspond to the distance between the geometrical centers of the [Au_3Cl_3] fragment and the Tr ligands

be compared with the total $[Au_3Cl_3Tr_2]^{2+}$ compound, which has also singlet multiplicity. The Au_3 fragment was calculated with charge +3 to preserve the Au(I) oxidation state that was adopted in the total complex. Table 2 shows the charge population of the Au_3^{+3} fragment, the s orbital population for Au2 and Au3 atoms (see Fig. 1) is about 2.8e, while for the Au1 atom it is smaller and equal to 2.3e. Further, the 5 d^{10} closed shell structure of the gold atoms underwent some changes: The $d_x{}^2{-}_y{}^2$ and $d_z{}^2$ orbitals present an electron population of 1.7 and 1.3e, respectively, in the Au2 and Au3 atoms. The breaking of the d^{10} structure in the gold atoms leads to a d–d interaction that combines with the s orbital mixing in the Au1 atom, and gives as a consequence the bonding observed in the Au_3^{+3} fragment. The latter can also be inferred from the spatial representation of the frontier molecular orbitals, which are depicted in Fig. 2: The HOMO is mainly made of the combination of the s and $d_z{}^2$ orbitals of gold. The LUMO is composed of antibonding $d_z{}^2$ orbitals located at the Au2 and Au3 atoms, with a smaller contribution of a d_{xz} orbital on the Au1 atom.

The fragment [Au_3Cl_3] was also calculated on singlet state, the orbital population for this fragment also shows a filling of the s orbitals and the 5 d^{10} electronic structure of the Au atoms is clearly reduced to about 9.6e (see Table 2). This is specifically observed on the $d_x{}^2{-}_y{}^2$ orbital of the three gold atoms, where an orbital population of 1.8e for the Au1 atom and an orbital population of 1.6e for the Au2 and Au3 atoms is observed. This electron distribution also leads to a d–d bonding, where a mixing of s orbitals is involved.

Consequently, the frontier MO's for the [Au_3Cl_3] fragment are essentially the same than those of the Au_3^{+3}; the HOMO is composed of s orbitals with a mixing of the $d_z{}^2$ orbitals of the Au atoms, while the LUMO also presents an antibonding configuration of the $d_z{}^2$ orbitals of the atoms Au2 and Au3 with a combination of the p_x orbitals of the Cl atoms. This indicates that the Au–Au bonds present in the complex come from a d – d interaction where an s–s bonding interaction is also involved.

In the $[Au_3Cl_3Tr_2]^{2+}$ total complex, the s electron population is slightly smaller than that found in the [Au_3Cl_3] fragment (see Table 2); in this case, the $d_x{}^2{-}_y{}^2$ electron populations for the three Au atoms is almost 2.0e, but the $d_z{}^2$ electron population is about 1.7e. This indicates that the $d_z{}^2$ orbitals participate in a bonding interaction in the total complex, which is different to the bonding in the [Au_3Cl_3] fragment.

According to the electron configuration of the Au atoms in the total complex, it is observed that the $5d^{10}6s^0$ closed shell structure is broken and goes to a $5d^{9.43}6s^{0.55}6p^{0.15}7s^{0.01}6d^{0.06}7p^{0.01}$, $5d^{9.52}6s^{0.61}6p^{0.09}7s^{0.01}6d^{0.05}7p^{0.01}$ and $5d^{9.52}6s^{0.61}6p^{0.09}7s^{0.01}6d^{0.05}7p^{0.01}$ electronic configurations for the Au1, Au2 and Au3 atoms, respectively. This

Table 2 Charge population according to NBO and Mülliken methods

	NBO population analysis								
	Charge population of Au_3^{3+}			Charge population of $[Au_3Cl_3]$			Charge population of $[Au_3Cl_3Tr_2]^{2+}$		
	Au1	Au2	Au3	Au1	Au2	Au3	Au1	Au2	Au3
S	2.274	2.780	2.781	3.024	2.565	2.577	2.553	2.608	2.608
p_x	2.045	2.022	2.021	2.025	2.019	2.018	2.084	2.035	2.035
p_y	2.012	2.046	2.046	2.020	2.036	2.035	2.044	2.036	2.037
p_z	2.008	2.007	2.007	2.015	2.013	2.012	2.016	2.012	2.012
d_{xy}	1.928	2.048	2.049	1.905	1.964	1.966	1.977	1.961	1.963
d_{xz}	1.991	1.991	1.991	1.974	1.988	1.986	1.956	1.942	1.937
d_{yz}	1.997	1.998	1.997	1.997	1.997	1.997	1.907	1.985	1.983
$d_{x^2-y^2}$	1.990	**1.688**	**1.660**	**1.832**	**1.645**	**1.643**	1.956	1.950	1.949
d_{z^2}	1.997	**1.300**	**1.325**	1.988	1.974	1.974	**1.687**	**1.735**	**1.742**
Total orbital d population	9.903	9.025	9.022	9.696	9.568	9.566	9.483	9.573	9.574
Mülliken charge population of $[Au_3Cl_3Tr_3]^{2+}$									
	Au1	Au2	Au3						
6s	0.76	0.75	0.76						
6p	0.65	0.77	0.65						
5d	-0.62	-0.67	-0.62						
5f	0.0008	0.001	0.0008						
Q_{Au}	0.21	0.15	0.21						

shows that the partial filling of the 6s shell is also the responsible for the aurophilic bonding in the central cluster.

Mülliken charges It is known that Mülliken population analysis gives no reliable absolute values; nevertheless, we report the results obtained from this approach at the VWN/TZP level, since the relative trend is in good agreement with the values given by the NBO method which were presented for the MP2 ground state geometry. The Mülliken population for the Au atoms and their corresponding valence orbitals at the VWN/TZP level are presented in Table 2. The valence 6 s and 6 p shells are populated from 0.65 to 0.77 electrons, while the 5 d shell presents a hole of about 0.60 e. The breaking of the closed shell electronic structure of the Au(I) cations is indicative of the presence of aurophilic bonding, where the empty Au6s and Au6p valence orbitals appear partially filled. The latter is in agreement with the results found with the NBO formalism at the MP2/B1 level.

We also considered another criterion to test the reliability of DFT on the study of aurophilic interactions; the difference between the molecular electron density and the sum of the atomic ground state densities, i.e., $\Delta\rho = \rho_{mol} - \sum\rho_{atom}$. A contour diagram of the density difference on the Au_3 plane is depicted in Fig. 3. The density distribution gives us an insight of the chemical nature on the bonding and non-bonding interactions, $\Delta\rho$ is used to highlight that information in more detail. An electronic density increasing (see Fig. 3) that ranges from +0.0067 to +0.047 e/Å^3 is observed in the overlapping region among the Au atoms, indicating that an orbital interference coming from the partial filling of the valence 6 s and 6 p shells is present, which induces a weak covalent bonding.

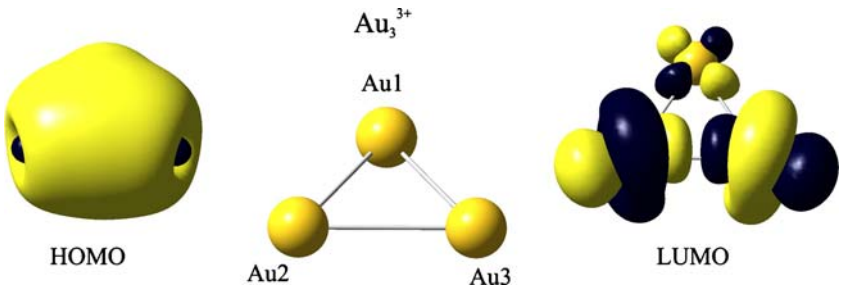

Fig. 2 Spatial representation of the frontier molecular orbitals for the fragment molecule Au_3^{3+}

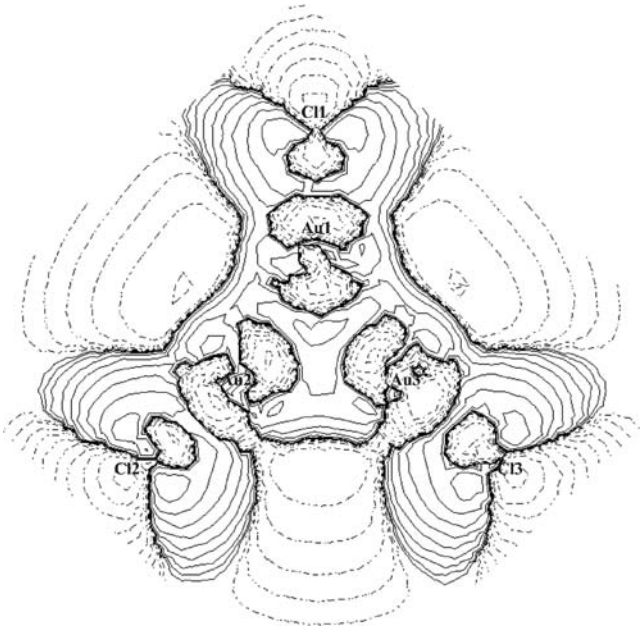

Fig. 3 Contour plot of the electronic difference density ($\Delta\rho$) of compound **1** in the plane of the Au_3Cl_3 monolayer sheet. The solid lines represent regions where the electron density is increased, while the dashed lines represent regions where the density is decreased

Donation and back-donation interactions

A CDA study (charge decomposition analysis) [46] has been carried out on the MP2 optimized geometry. This analysis gives us a picture of the donor-acceptor interactions partitioning into two fragments the complex under study. The method builds the wave function of the complex considering the linear combination of the donor and acceptor fragment orbitals (LCFO). CDA returns the following contributions: Charge donation from the occupied orbitals of the donor to the unoccupied orbitals of the acceptor, back-donation from the occupied orbitals of the acceptor to the unoccupied orbitals of the donor, and the repulsive polarization; which accounts for the charge removed from the overlapping area of the occupied orbitals of the donor and acceptor fragments.

The CDA results show that the amount of charge donation from the Tr ligands to the gold central cluster is small compared to the back-donation from the $[Au_3Cl_3]$ fragment to the Tr ligands. The HOMO-3, HOMO-5 and HOMO-6 (Molecular Orbitals 99, 97 and 96, respectively) can be considered the most important contributions to the donating character; since those MO's donate 0.679e into the bonding region from the Tr ligands. Summing over all the contributions from the occupied MO's to the donation interaction, a total of −7.38e is obtained, which indicates that no significant donating character is involved in the bonding of complex (1). This assumption can be corroborated from the contour diagrams depicted in Fig. 4 of the HOMO-3, HOMO-5 and HOMO-6, that do not show a significant charge contribution in the bonding region, since the charge mainly resides on the Cl atoms.

On the other hand, the back-donation is much stronger in complex (1), since according to the CDA results, a total of +2.62e is transferred into the bonding region from the gold ring. The back donation interaction may be addressed to the highest-energy MO's where the contribution is larger, such as HOMO-9, HOMO-10 and HOMO-11; in these MO's a large charge contribution in the bonding region is present, as seen on Fig. 4. The repulsive polarization term in the CDA analysis can not be neglected: A total value of +2.447e is returned; this contribution can be interpreted as the amount of charge that remains in the overlapping region of the occupied MO's of the donor-acceptor fragments, giving as a result the slight deformation on the planarity of the Tr ligands, as seen from the lateral view in Fig. 1.

Bonding energy

The bonding among the Tr ligands and the trigold(I) compound was also studied using DFT with the VWN functional. The latter was carried out with an energy decomposition analysis according to the technique developed by Ziegler [47, 48]; the energy is partitioned in three contributions: The Pauli repulsion energy, the electrostatic attraction and the orbital relaxation. To compute the first two terms, the trigold(I) compound and the Tr ligands are taken as two separate fragments, where their MO's remain unchanged, the Pauli repulsion refers to the increment in kinetic energy of uncoupled electrons, resulting from the Pauli principle (E_{Pauli}). The electrostatic attraction is the attractive electrostatic overlap interacion (E_{elec}); when summing over the last two terms, the steric energy term is returned.

Finally, the orbital relaxation is obtained by mixing the occupied and unoccupied MO's of the trigold(I) and Tr ligands fragments; at this step, the charge transfer and the polarization contributions are involved: The former term comes from the electronic population transferred from the occupied orbitals of one fragment to the virtual orbitals of the other fragment; in the latter term, the transference comes from the occupied orbitals of one fragment to its own virtual orbitals. The energy break-down of complex (1) is presented in Table 3. The electrostatic attraction is overcome by the Pauli repulsion giving as a result a repulsive steric energy of +413 kcal mol^{-1}. The whole complex becomes bound when the orbital relaxation is involved, with a contribution of −587 kcal mol^{-1} coming from orbital mixing. The sum of all terms induces a stabilized total energy that amounts to -174 kcal mol^{-1}.

On the other hand, the HOMO-LUMO gap reported by Murahashi et al. [7] for the $[Pd_3Cl_3Tr_2]^-$ compound amounts to 3.0 eV at the B3LYP/TZVP level of theory; while the gap calculated in this work for complex (1) at the

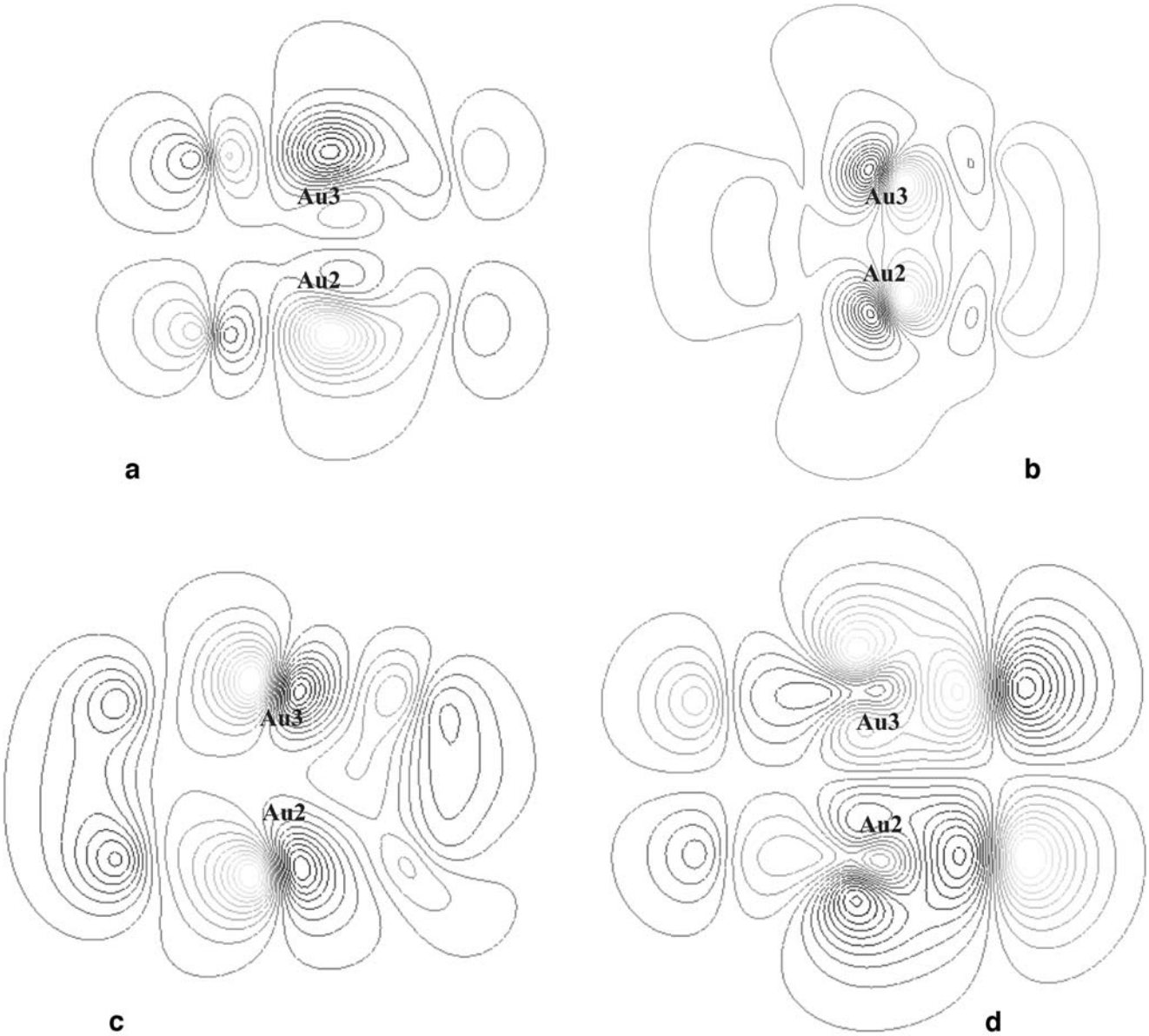

Fig. 4 Contour plots of some orbitals of compound **1** at MP2/B1.The plots lie on the perpendicular direction to the plane of the gold monolayer sheet: (**a**) HOMO-3; (**b**) HOMO-5, (**c**) HOMO-9; (**d**) HOMO-10

B3LYP/TZVP//MP2/B1 level is 2.5 eV, indicating that it would have a higher reactivity. Considering that the Palladium complex presents catalytic properties, an analogous behavior would be expected from the gold sandwich compound, since the gap size is comparable to that of the Pd compound.

Table 3 Bond energy decomposition of complex **1** using ZORA at the VWN level

Energy contribution	kcal mol^{-1}
Pauli repulsion energy(1)	+995.57
Electrostatic attraction	−582.32
Steric energy	**+413.25**
Orbital relaxation(2)	−587.39
Total bonding energy	**-174.14**

Aromaticity

Magnetic shieldings were computed to find the nuclear independent chemical shift (NICS) in accordance to the Schleyer's method [38]. NICS calculations were performed at the center of the Tr ligands and at the center of the $[Au_3Cl_3]$ monolayer sheet considering the MP2/B1 ground state geometry. Those values are reported in Fig. 1; the NICS values at the center of the Tr ligands indicate aromaticity, the NICS value at the center of the $[Au_3Cl_3]$ cluster shows a stronger aromatic character. Since the NICS

value at the center of the compound is greater than those at the center of the rings, the stability and aromatic character of the full compound may be expected.

The aromatic behavior of complex (1) was also studied using the harmonic oscillator model of aromaticity (HOMA) [39], which is one of the main geometric models. It was adopted to quantify the aromatic character of the cycloheptatrienyl ligands. If we consider heterocyclic rings, the definition of HOMA is given by:

$$HOMA = 1 - \frac{1}{n}\alpha \sum \left(R_{opt,j} - R_{ij}\right)^2$$

where n is the number of all bonds, j represents bond type, α is a normalization factor that takes into account a value of HOMA=0 for the hypothetical Kekulé structure and HOMA=1 if the complex is perfectly aromatic, i.e., a compound with all bonds of *j*th type equal to the optimal length $R_{opt,j}$, while for benzene the HOMA is 0.988; finally, $R_{i,j}$ is the *i*th bond distance of *j*th type. The constants $R_{opt,j}$ and α for the carbon-carbon bond [39] amounts to $R_{opt,j}$= 1.397 Å and α=257.7 $Å^{-1}$; these parameters were employed in the calculation of the aromatic character of the Tr ligands.

The HOMA value for benzene was used as a reference point to be compared with the calculated HOMA values for the Tr fragments. In accordance with HOMA, benzene is 100% aromatic, and a smaller value is indicative of a decreasing on the aromatic character. The HOMA values indicate that the upper and lower Tr ligands have an 82 and an 81%, respectively, of the aromatic character of benzene. These results are in agreement with those found with the NICS values at the center of the cycloheptatrienyl ligands.

On the other hand, NICS calculations were performed at the VWN/TZP computational level at exactly the same locations as those computed by the MP2 computational method (see Fig. 1). The NICS values on the Tr ligands are smaller than that on the trigold(I) sheet, which gives a strong aromatic character to the whole molecule. These results are in good agreement with those found at the MP2/B1 level.

Conclusions

The existence of the sandwich compound with an Au monolayer sheet $[Au_3Tr_2Cl_3]^{2+}$ has been predicted at the ab-initio level of theory and at the scalar relativistic DFT. The bonding between the Tr^+ ligands and the gold monolayer sheet is mainly governed by an electron back-donation interaction coming from the central gold sheet to the Tr^+ ligands with slight contributions originating from electron donation. The Au–Au bond lengths inside the central gold sheet are in the range of aurophilic interactions; such bonding is ruled by a d–d interaction where the 5 d shell is no longer inert and the closed-shell structure of the Au(I) cations is broken, triggering the partial filling of the 6sp shell, contributing to the rise of the aurophilic bonding. The overall stabilization of complex (1) can be inferred from the strong aurophilic interaction observed in the metal sheet and from the strong aromatic character in the whole molecule.

A chemical difference density of about +0.047 e/$Å^3$ among the interacting gold atoms inside the ring, revealed that the aurophilic interaction contains a weak covalent Au–Au bonding; the latter can also be addressed to the breaking of the closed Au 5d shell and the partial filling of the Au 6sp shell, according to Mülliken orbital populations at the VWN/TZP level. The observed increasing on overlap interference density at the region among the metal centers may be considered as enough to reproduce reasonable electron correlation energies. Consequently, the use of DFT may be considered a reliable choice for the study of the aurophilic attraction, since dispersion is not the only phenomenon involved in the interaction.

Acknowledgements The authors wish to thank the Impulsa Project, PUNTA, PAEP-UNAM, PAPIIT-IN107807 and DGSCA – UNAM for providing computing time. J. Muñiz acknowledges the financial support of the Consejo Nacional de Ciencia y Tecnología (CONACyT), under fellowship No. 180250.

References

1. Wilkinson G, Rosenblum M, Whiting MC, Woodward RB (1952) J Am Chem Soc 74:2125–2126
2. Beck V, O'Hare D (2004) J Organomet Chem 689:3920–3938
3. Kurikawa T, Takeda H, Hirano M, Judai K, Arita T, Nagao S, Nakajima A, Kaya K (1999) Organometallics 18:1430–1438
4. Mireles N, Sansores LE, Martínez A, Salcedo R (2003) Int J Quantum Chem 94:51–56
5. Mireles N, Salcedo R, Sansores LE, Martínez A (2000) Int J Quantum Chem 80:258–263
6. Burdett JK, Canadell E (1985) Organometallics 4:805–815
7. Murahashi T, Fujimoto M, Oka M, Hashimoto Y, Uemura T, Tatsumi Y, Nakao Y, Ikeda A, Sakaki S, Kurosawa H (2006) Science 313:1104–1107
8. Pyykkö P (1997) Chem Rev 97:597–636
9. Sansores LE, Salcedo R, Flores H, Martínez A (2000) J Mol Struct (Theochem) 530:125–129
10. Muñiz J, Sansores LE, Martínez A, Salcedo R (2007) J Mol Struct (Theochem) 820:141–147
11. Sansores LE, Salcedo R, Martínez A (2004) J Mol Struct (Theochem) 677:145–151
12. Schmidbaur H (1995) Chem Soc Rev 24:391–400
13. Mingos DMP (1996) J Chem Soc, Dalton Trans 5:561–566
14. van Zyl WE, López-de-Luzuriaga JM, Fackler Jr JP (2000) J Mol Struct 516:99–106
15. Li J, Pyykkö P (1992) Chem Phys Lett 197:586–590
16. Pyykkö P, Li L, Runeberg N (1994) Chem Phys Lett 218:133–138
17. Pyykkö P (2002) Angew Chem Int Ed Engl 41:3573–3578

18. Schwerdtfeger P (2003) Angew Chem Int Ed Engl 42:1892–1895
19. Møller C, Plesset MS (1934) Phys Rev 46:618–622
20. Hay PJ, Wadt WR (1985) J Chem Phys 82:299–310
21. Andrae D, Haeussermann U, Dolg M, Stoll H, Preuss H (1990) Theor Chim Acta 77:123–141
22. Schäfer A, Huber C, Ahlrichs RJ (1994) Chem Phys 100:5829
23. Pyykkö P, Runeberg N, Mendizabal F (1997) Chem Eur J 3:1451–1457
24. Petersson GA, Al-Laham MA (1991) J Chem Phys 94:6081–6090
25. Petersson GA, Bennett A, Tensfeldt TG, Al-Laham MA, Shirley WA, Mantzaris J (1988) J Chem Phys 89:2193–2218
26. NBO Version 3.1, Glendening ED, Reed AE, Carpenter JE, Weinhold F
27. Slater JC (1951) Phys Rev 81:385–390
28. Gaspar R (1954) Acta Phys Acad Sci Hung 3:263–286
29. Schwarz K (1972) Phys Rev B 5:2466–2468
30. Vosko SH, Wilk L, Nusair M (1980) Can J Phys 58:1200–1211
31. Becke AD (1988) J Chem Phys 88:2547–2553
32. Perdew JP (1986) Phys Rev B 33:8822–8824
33. Te Velde G, Baerends EJ (1992) J Comput Phys 99:84–98
34. Te Velde G, Bickelhaupt FM, Baerends EJ, Guerra CF, Van Gisbergen SJA, Snijders JG, Ziegler T (2001) J Comput Chem 22:931–967
35. van Lenthe E, Baerends EJ, Snijders JG (1994) J Chem Phys 101:9783–9792
36. (a) van Lenthe E (1996) Int J Quantum Chem 57:281–293 (b) van Lenthe E, Ehlers AE, Baerends EJ (1999) J Chem Phys 110:8943–8953
37. van Lenthe E, Snijders JG, Baerends EJ (1996) J Chem Phys 105:6505–6516
38. Schleyer PvR, Maerker C, Dransfeld A, Jiao H, Hommes NJvE (1996) J Am Chem Soc 118:6317–6318
39. Krygowski TM (1993) J Chem Inf Comput Sci 33:70–78
40. Frisch MJ, Trucks GW, Schlegel HB, Scuseria GE, Robb MA, Cheeseman JR, Montgomery JA, Vreven Jr T, Kudin KN, Burant JC, Millam M, Iyengar SS, Tomasi J, Barone V, Mennucci B, Cossi M, Scalmani G, Rega N, Petersson GA, Nakatsuji H, Hada M, Ehara M, Toyota K, Fukuda R, Hasegawa J, Ishida M, Nakajima T, Honda Y, Kitao O, Nakai H, Klene M, Li X, Knox JE, Hratchian HP, Cross JB, Adamo C, Jaramillo J, Gomperts R, Stratmann RE, Yazyev O, Austin J, Cammi R, Pomelli C, Ochterski JW, Ayala PY, Morokuma K, Voth GA, Salvador P, Dannenberg JJ, Zakrzewski VG, Dapprich S, Daniels D, Strain MC, Farkas O, Malick DK, Rabuck D, Raghavachari K, Foresman JB, Ortiz JV, Cui Q, Baboul G, Clifford S, Cioslowski J, Stefanov BB, Liu G, Liashenko A, Piskorz P, Komaromi I, Martin RL, Fox DJ, Keith T, Al-Laham MA, Peng CY, Nanayakkara A, Challacombe M, Gill PMW, Johnson B, Chen W, Wong MW, Gonzalez C, Pople JA (2004) Gaussian 03, Revision D.01. Gaussian Inc, Wallingford CT
41. Fonseca-Guerra C, Snijders JG, Te Velde G, Baerends EJ (1998) Theor Chem Acc 99:391–403
42. ADF2006.01, SCM, Theoretical Chemistry, Vrije Universiteit, Amsterdam, The Netherlands, http://www.scm.com
43. Herschbach DR, Laurie VW (1961) J Chem Phys 35:458–464
44. Wiberg KB (1968) Tetrahedron 24:1083–1096
45. Wang S-G, Schwarz WHE (2004) J Am Chem Soc 126:1266–1276
46. Dapprich S, Frenking G (1995) J Phys Chem 99:9352–9362
47. Ziegler T, Rauk A (1977) Theor Chim Acta 46:1–10
48. Ziegler T, Rauk A, Baerends EJ (1977) Theor Chim Acta 43:261–271